To be presented at: Faraday Discussion 84: Dynamics of Elementary Gas Phase Reactions, 14-16 September 1987, University of Birmingham, Birmingham, ENGLAND

INSIGHTS INTO THE MECHANISMS OF CHEMICAL REACTIONS: REACTION PATHS FOR CHEMICAL REACTIONS

Thom H. Dunning, Jr., Elfi Rosen, and Robert A. Eades

Theoretical Chemistry Group, Chemistry Division
Argonne National Laboratory, Argonne, Illinois, USA 60439

The concept of a *reaction path* which continuously describes the transformation of reactants to products is firmly embedded in the *lore* of chemistry. A formal definition of the reaction path for a general molecular system was proposed by Fukui in 1970 as the path of steepest descent in mass-weighted cartesian coordinates from the transition state to reactants in one direction and to products in the other. In 1980 Miller, Handy & Adams put forward a formal theory of reaction dynamics based on harmonic flucuations about the reaction path. We report reaction paths for two prototypical chemical reactions: Li + HF, an electron transfer reaction, and OH + H_2, an abstraction reaction. In the first reaction we consider the connection between the energetic terms in the reaction path Hamiltonian and the electronic changes which occur upon reaction. In the second reaction we consider the treatment of vibrational effects in chemical reactions in the reaction path formalism.

ional

path

barrier height[4(b,d)]. They have also calculated reaction paths for a few simple reactions and discussed the qualitative features of these reactions in terms of the calculated paths[5].

In 1980 Miller, Handy & Adams [6] used the definition of the reaction path given by Fukui[3] along with the approach of Hougen, Bunker & Johns[7] to develop a formal theory for treating the dynamics of reactions involving polyatomic species. In this formalism the large amplitude mode in the theory of molecular vibrations advanced by Hougen, Bunker & Johns[7] just corresponds to motion along the reaction path. The *reaction path Hamiltonian* approach of Miller, Handy & Adams requires that the potential energy surface be specified only in the immediate vicinity of the reaction path and, thus, provides an approach readily applicable to systems with four or more atoms. Miller, Schaefer & coworkers have also reported reaction paths for a number of simple reactions.[8]

In the following section we review the reaction path formalism as developed by Miller, Handy & Adams[6], focusing on the terms in the reaction path Hamiltonian which explicitly depend on the potential energy surface. We then discuss two examples chosen to illustrate different aspects of the description of chemical reactions in the reaction path formalism. The first, an electron transfer reaction: Li + HF, shows the intimate connection between the energetic terms in the reaction path Hamiltonian and the electronic changes resulting from chemical reaction. The second, an abstraction reaction: OH + H_2, focuses on the description of vibrational effects on reactions. Here we consider not only the energetic terms in the Hamiltonian but also the dynamical terms explicitly coupling the various modes in the system as a result of motion along the reaction path. These terms are necessary to fully describe the effect of vibrational excitation of the reagents on the rate of the reaction.

2. THE REACTION PATH HAMILTONIAN

While insights into the qualitative features of chemical reactions may be gained just by calculating the reaction path, in order to develop a detailed understanding of the mechanism, energetics and dynamics of reactions, information on the potential energy surface is also required. Miller, Handy & Adams[6] proposed to characterize a reacting system *via* the reaction path coupled with harmonic fluctuations about it, or in order words, to approximate the most critical portion of the potential energy surface as a many dimensional *harmonic valley* centered on the reaction path; this is illustrated schematically in Fig. 1. We shall refer to this region as the *reaction valley*.

To calculate the reaction valley, we need to first determine the steepest descent path in mass-weighted cartesian coordinates down from the saddle point to reactants in one direction and to products in the other direction.[3] The steepest descent path is computed by following the gradient of the energy with the first step taken in the direction of the reaction coordinate at the saddle point. Efficient algorithms exist both for computing the gradient of a Born-Oppenheimer potential energy surface, $V(\underline{x})$[9], and for following the minimum energy path.[10] The reaction path $\underline{x}_S(s)$ is a parametric function of the reaction coordinate s (the mass-weighted cartesian distance along the path); it is determined by:

$$(d/ds)\, x_{si}(s) = [-\partial V(\underline{x})/\partial x_i]/\,|\,\partial V(\underline{x})/\partial x_i\,| \qquad (1)$$

where x_i refers to one of the nuclear cartesian coordinates. In addition, one requires the force constant matrix, K(s), along the reaction path with:

$$K_{ij}(s) = [\partial^2 V(\underline{x})/\partial x_i \partial x_j]_{\,x=x_S(s)} \qquad (2)$$

Diagonalization of the force constant matrix yields the eigenvectors $\mathbf{L} = \{L_k(s)\}$, the

normal modes $\mathbf{Q} = \{Q_k(s)\}$ and the harmonic frequencies $\omega = \{\omega_k(s)\}$ for the 3N-7 local motions orthogonal to the reaction path $\underline{x}_s(s)$; six zero eigenvalues are also obtained[11] - these correspond to translation and rotation of the molecular system as a whole.

The molecular system can now be described in terms of the set of 3N-6 reaction path coordinates, namely, the reaction coordinate, $\underline{x}_s(s)$, and the 3N-7 local modes, $\mathbf{Q}(s)$. In this coordinate system the cartesian coordinates $\underline{x}$ of a general point in configuration space are represented by the cartesian coordinates of a point $\underline{x}_s(s)$ on the reaction path plus the 3N-7 displacements $\mathbf{Q}(s)$ orthogonal to the path:[11]

$$\underline{x} = \underline{x}_s(s) + \sum_k L_k(s)\, Q_k(s) \tag{3}$$

In terms of the reaction path coordinates, (s, $\mathbf{Q}$), and their conjugated momenta, (p_s, $\mathbf{P}$), the molecular Hamiltonian $\mathcal{H}(s,p_s,\mathbf{Q},\mathbf{P})$ is defined by:

$$\mathcal{H}(s,p_s,\mathbf{Q},\mathbf{P}) = T(s,p_s,\mathbf{Q},\mathbf{P}) + V(s,\mathbf{Q}) \tag{4}$$

In the approach of Miller, Handy and Adam,[6] the potential energy is approximated at each point s by the potential energy at that point on the path plus the potential energy for harmonic displacements perpendicular to the path:

$$V(s,\mathbf{Q}) = V_s(s) + {}^1/_2 \sum_k \omega_k(s)^2\, Q_k(s)^2 \tag{5}$$

The kinetic energy portion of the Hamiltonian for a system with zero angular momentum is given exactly by:

$$T(s,p_s,\mathbf{Q},\mathbf{P}) = {}^1/_2 \left[p_s - \sum_k Q_k(s) P_{k'}(s) B_{kk'}(s)\right]^2 / \left[1 + \sum_k Q_k(s) B_{ks}(s)\right]^2 + {}^1/_2 \sum_k P_k(s)^2 \tag{6}$$

As can be seen in (5) and (6), there are two types of terms in the reaction path Hamiltonian which depend on the potential energy surface: the energy terms, $V_s(s)$ and $\omega_k(s)$, and the coupling terms, $B_{ks}(s)$ and $B_{kk'}(s)$. A detailed description of the effect of the dynamics of chemical reactions requires the consideration of both terms. Let us consider the energy terms first. Within the framework of the reaction path Hamiltonian, the effective potential for motion along the reaction path is:

$$V_{vap}^{n}(s) = V_s(s) + V_{vib}^{n}(s) \tag{7}$$

where $V_{vib}^{n}(s)$ is the total energy of the bound vibrational modes *relative* to the energy of the corresponding state in the reactants; this is just the vibrationally adiabatic potential. Within the harmonic approximation $V_{vib}^{n}(s)$ is:

$$V_{vib}^{n}(s) = \hbar \sum_k (n_k + 1/2) [\omega_k(s) - \omega_k(s=-\infty)] \tag{8}$$

for the vibrational state defined by the quantum numbers $\mathbf{n} = (n_1,n_2,...,n_{3N-7})$. For the case $\mathbf{n} = (0,0,...,0)$, $V_{vib}^{0}(s)$ is the ground state adiabatic potential and $V_{vib}^{0}(s)$ is the *change* in the zero point energy. The vibrationally adiabatic threshold for reaction is the maximum on the vibrationally adiabatic potential (which, in general, will not be located at the saddle point[12]).

Given the dependence of the vibrational frequencies on the reaction coordinate, s, the energetic effect of vibrational excitation can be calculated from (7). Clearly, if the frequency of one (or more) of the modes decreases significantly as the reaction proceeds, $[\omega_k(s) - \omega_k(s=-\infty)]$ will be negative and vibrational excitation of this mode will lead to a reduction in the threshold for the reaction and a corresponding increase in the reaction rate.

The dynamical coupling between motion along the reaction path and the

transverse vibrations is reflected in the coupling terms, $B_{ks}(s)$ and $B_{kk'}(s)$ appearing in the kinetic energy expression. The $B_{ks}(s)$ term

$$B_{ks}(s) = [\partial \underline{L}_k(s)/\partial s] \cdot \underline{x}_s(s) \quad (9)$$

describes the direct coupling between the reaction path s and vibrational mode k. It is a measure of the mixing between vibrational mode k and the reaction path induced by the curvature of the reaction path. The total curvature of the reaction path is defined as:

$$\kappa(s) = [\sum_k B_{ks}(s)2]^{1/2} \quad (10)$$

The $B_{ks}(s)$ terms are referred to as *curvature couplings*. The $B_{kk'}(s)$ term

$$B_{kk'}(s) = [\partial L_k(s)/\partial s] \cdot L_{k'}(s) \quad (11)$$

describes the mixing between modes k and k' induced by the motion of the system along the reaction path. As this motion involves a twisting of the vibrational modes about the reaction path, the $B_{kk'}(s)$ terms are referred to as *coriolis couplings*.

The coupling terms provide a dynamical measure of the adiabaticity of the reaction. If the coupling terms are negligible, the equation for motion along the path reduces to:

$$[1/2 p_s^2 + V_{vap}^n(s)]\chi_i(s) = E\chi_i(s) \quad (12)$$

for vibrational state n. In (12) $\chi_i(s)$ is the scattering wavefunction. That is, the potential for motion along the path is simply the adiabatic potential (7). In this case the effect of vibrational energy on the reaction is determined by the energetic terms alone. If, on the other hand, the B_{ks} and $B_{kk'}$ are not negligible, then motion along

the reaction path is dynamically coupled to the transverse vibrations. Energy flow between the reaction coordinate and the vibrational modes will depend on the relative translational energy of the reactants, the magnitude of the coupling terms, *etc.* Of course, if the coupling terms become sufficiently large, the reaction path approach itself breaks down because of the presence of singularities in the kinetic energy expression, *i.e.*, $[1+\Sigma_k Q_k(s)B_{ks}(s)]^{-1} \rightarrow \infty$ for points on the potential energy surface very close to the reaction path.

As a result of the harmonic approximation to the potential energy, the frequencies $\{\omega_k(s)\}$ obey a non-crossing rule, *i.e.*, frequencies corresponding to modes of the same symmetry do not cross. If all $B_{kk'}$ values are zero, there is no interaction between the transverse modes, and their character is preserved during the course of the reaction. On the other hand, if there is a strong interaction, as in the case of an avoided crossing, the $B_{kk'}$ values become large in magnitude. In this case, the extent of mixing of the two modes will depend on the energy splitting between the two modes, the nature of the coupling term and the relative translational energy of the species involved. This situation is analogous to breakdowns in the Born-Oppenheimer approximation induced by (avoided) crossings of electronic states. We shall see an example of this behavior in the OH + H_2 reaction.

3. An Electron Transfer Reaction, Li + HF: Electronic Effects in Chemical Reactions[13]

The reaction of an alkali atom with a hydrogen halide molecule to form an alkali halide molecule has played a central role in the development of chemical dynamics. The first successful molecular beam experiment was of the K + HBr system.[14] Studies by other workers has shown that these reactions do not follow the standard harpooning mechanism as the electron jump occurs at small internuclear separation of the reactants.[15] Nonetheless, as we shall see, the alkali-hydrogen halide reactions provide a stunning example of the influence of electronic effects on chemical

reactions - transfer of the electron from the incoming alkali atom to the departing hydrogen causes dramatic changes in the reaction path Hamiltonian.

We report here a calculation of the reaction path for the reaction of lithium atom with hydrogen fluoride:

$$Li + HF \rightarrow LiF + H \qquad (13)$$

Two *ab initio* theoretical calculations[16] have been reported on the potential energy surface for reaction (13); this work has been complimented by a detailed molecular beam study[17] of this reaction and the analogous Li + HCl reaction. The theoretical calculations of Chen & Schaefer[16(b)] predicted a well 4.6 kcal/mol deep in the entrance channel at an LiFH angle of 114° and a barrier 10.0 kcal/mol high at an LiFH angle of 74° located in the exit channel (the molecular beam measurements[17] suggest that the calculated barrier height is 2-4 kcal/mol too high). From a visual examination of a series of slices of the potential energy surface, Chen & Schaefer[16(b)] concluded that the reaction proceeded by an unusual *backside attack-barrier-backside exit* mechanism, *i.e.*, the lithium atom approaches the hydrogen atom from the fluorine side and then, after surmounting the barrier, exits the transition state region by again swinging around behind the fluorine.

The calculation of the reaction path of (13) reported here was carried out at essentially the same calculational level as Chen & Schaefer[16(b)] in order that a direct comparison could be made to their results. The geometries and energies of the reactants, Li·· FH complex, saddle point and products were, as expected, the same as those found in the previous study. The reaction path, however, was directly calculated by following the steepest descent path from the saddle point as outlined in the previous section.

The geometry of the system along the reaction path is plotted in Fig. 2. The lithium atom initially approaches the fluorine end of the HF molecule, forming a

weakly bound dipole-induced dipole complex. While a dipole-induced dipole interaction favors a collinear configuration of the atoms, the distribution of the lone pair electrons around the fluorine atom leads to a bent geometry with a LiFH angle, θ_{LiFH}, of 114°. This bound complex is located in the entrance channel with a calculated lithium-fluorine distance, R_{LiF}, of 1.95Å (0.35Å longer than in the isolated LiF molecule) and a fluorine-hydrogen distance of 0.94Å (negligibly longer than in the hydrogen fluoride molecule). From the complex to the saddle point, R_{LiF} decrease from 1.95Å to 1.70Å while θ_{LiFH} decreases from 114° to 75°. The most dramatic change occurs in R_{FH}. Over this region, the fluorine-hydrogen separation remains essentially constant until s ≈ -25 au; it then sharply increases becoming coincident with the reaction path by the time the saddle point is reached. After the saddle point the reaction path simply corresponds to ejection of the hydrogen atom. The saddle point is located in the exit channel with R_{LiF} just 0.09Å longer than in lithium fluoride.

The cause of the dramatic change in R_{FH} is seen in the plots of the singly orbital of the LiFH complex at selected points along the reaction path in Fig. 3. At s ≈ -25 au the singly occupied orbital, which was essentially a polarized 2s-orbital centered on the lithium atom, begins to delocalize onto the hydrogen atom. The transfer of the electron from the lithium atom to the hydrogen atom then rapidly takes place, being essentially complete by the time the saddle point is reached. It is this rapid transfer of the electron from the lithium atom to the hydrogen atom which causes the change in the fluorine-hydrogen distance so dramatically illustrated in Fig. 2.

This rapid transfer of the electron from the lithium atom to the hydrogen atom has an even more pronounced effect on the vibrational frequencies of the bound modes along the reaction path as illustrated in Fig. 4. From the reactants through the Li···FH complex there is little change in the FH stretching frequency from its calculated frequency of 3905 cm^{-1} in the isolated molecule and only a gradual increase in the LiFH bending frequency. At s ≈ -25Å the HF stretching frequency plummets; at the saddle point the highest frequency mode is just 840 cm^{-1}. This

dramatic drop in the FH vibrational frequency is a direct result of the destruction of the FH bond caused by the electron transfer.

The decrease in the HF vibrational frequency along the reaction path has an important effect on the energetics of (13) as can be seen in Fig. 5. The calculated ground state vibrationally adiabatic barrier is more than 3 kcal/mol *lower* than the classical barrier. We have also plotted the vibrationally adiabatic potential for Li + HF(n_{HF}=1) in Fig. 5. The calculations predict that there will be **no** barrier for reaction of vibrationally excited hydrogen fluoride. Hence, the rate of (13) should be strongly enhanced by vibrational excitation of the hydrogen halide. The effect of vibrational excitation on (13) has not yet been measured. However, for the analogous K + HCl reaction, Brooks & coworkers[18] have shown that vibrational excitation of the hydrogen halide is far more effective than an equivalent amount of translational energy in accelerating the rate of the reaction.

4. The Abstraction Reaction: OH + H_2. Vibrational Effects in Chemical Reactions [19]

The bimolecular reaction between OH and H_2 plays an important role in many chemical processes including hydrogen and hydrocarbon combustion and atmospheric chemistry. This reaction is the principal source of water production in hydrogen/oxygen flames[20] and is also known to be the main source of water in hydrocarbon air flames at atmospheric pressure.[21] Because of its singular importance, this reaction has received special attention by both experimentalists and theoreticians. Of particular interest here are the experimental studies of the enhancements in the rate constant of this reaction resulting from vibrational excitation of the reactants - measurements have been reported for vibrational excitation of both reagents.[22-24] As such, this reaction is an ideal test case for investigating the reaction path approach for describing vibrational effects in chemical reactions.

We report here a calculation of the reaction path for the reaction of hydroxyl radical with molecular hydrogen

$$OH(n_{OH}) + H_2(n_{H_2}) \rightarrow H_2O(n_1,n_2,n_3) + H \qquad (14)$$

including all of the terms in the reaction path Hamiltonian required to quantify the effects of vibrational excitation on the reaction.

Experimentally, for (14), Zellner *et al.*[24] report a rate enhancement for $H_2(n_{H_2}=1)$ of a factor of 80-160 at 300°K and Glass & Chaturvedi[22(b)] report a factor of 120-190 at 300°K. In contrast, Spencer, Endo & Glass[22(a)] found that vibrational excitation of OH increases the rate of (14) by less than a factor of two. This is so in spite of the fact that vibrationally excited OH has 10.2 kcal/mol more energy than $OH(n_{OH}=0)$. On the theoretical side, extensive dynamical studies of (14), primarily based on the global potential energy surface of Walch, Dunning, Schatz & Elgersma[25] have been performed. These studies have focused on determining the effect of vibrational excitation of reactants on the reaction rates and the product state energy distribution (see, for example, work by Schatz,[26] Truhlar & Isaacson,[27] or Rashed & Brown[28]). The conclusions drawn from these works are, of course, limited by the accuracy of the potential energy surface; a detailed analysis of this surface will be reported shortly.[19]

As noted in Section II, an understanding of vibrational effects in chemical reactions requires that we determine the changes in the vibrational frequencies, $\{\omega_k(s)\}$, and normal modes, $\{Q_k(s)\}$, along the reaction path. The calculated frequencies for (14) are plotted in Fig. 6; the vibrationally adiabatic potentials for $(n_{OH}=0,n_{H_2}=0)$, $(n_{OH}=1,n_{H_2}=0)$ and $(n_{OH}=0,n_{H_2}=1)$ are plotted in Fig. 7. Based on the experimental evidence Zellner & Steinert[24] estimated a decrease in the activation energy at 300°K of 3.4 kcal/mol. Vibrational excitation of the OH molecule has a negligible effect on the barrier. From Fig. 7 we find that vibrational excitation of the

OH molecule decreases the vibrationally adiabatic threshold by 0.3 kcal/mol while excitation of the H_2 molecule decreases the barrier height by 3.0 kcal/mol.[29] Even in the latter case, vibrational excitation is relatively ineffective in accelerating the rate of the reaction - less than one quarter of the additional vibrational energy in H_2 is effective in overcoming the barrier.

As noted in Section II, a detailed dynamical treatment of (14) requires, in addition to the vibrational frequencies, the terms coupling motion along the path with the vibrational motions orthogonal to the path, B_{ks} (s) and $B_{kk'}$(s). These terms govern the flow of energy between the bound modes and the reaction coordinate as the system moves along the reaction path from reactants through the transition state to products. As shown in Fig. 8, there is almost no coupling between the OH stretch and the reaction path in the entrance channel; the value of $B_{OH,s}$ is close to zero in that region. Thus, excitation of this bond does not enhance the rate of reaction because there is no way for the vibrational energy to flow into the reaction path (this is also reflected in the minor changes noted in ω_{OH}(s) in Fig. 6). The OH bond can thus be considered a *spectator* bond. The H_2 stretching mode, on the other hand, strongly couples with the reaction path in the entrance channel, attaining a maximum value just before the saddle point. Energy can flow from the H_2 stretch into the reaction path *via* the $B_{HH,s}$ coupling terms, and hence, excitation of this bond has a large effect on the reaction rate. This is not unexpected as it is the H_2 bond which is broken in the reaction. However, this simple rationale does not hold in all cases, *e.g.*, for the OH + HBr reaction, vibrational excitation of the OH accelerates the rate of reaction by an order of magnitude.[30]

Within the framework of the reaction path Hamiltonian approach, frequencies of the same symmetry do not cross. In Fig. 9 we focus on the region in the immediate vicinity of the avoided crossing of the OH and H_2 stretching modes. As noted in Section II, coriolis coupling terms are expected to be large in the vicinity of sharply avoided crossings. We have also plotted the $B_{OH,HH}$ term describing the coupling of the OH and the H_2 stretch along the reaction path in Fig. 9. As can be seen, there

is essentially no coupling between the OH and the H_2 stretch except near s ≈ -14 au, the location of the avoided crossing. At that point there is a sharp peak in the $B_{OH,HH}$ term which will induce a localized (diabatic) transition between the two adiabatic states. Hence, we conclude that it is physically more reasonable to assume that the OH and H_2 stretches preserve their character during the course of the reaction. Knowing this, we plotted the vibrational frequencies in Fig. 6 as if the curves for $\omega_{OH}(s)$ and $\omega_{H_2}(s)$ cross at s ≈ -14 au. This same assumption was also used to compute the vibrationally adiabatic potentials plotted in Fig. 7.

The influence of vibrational excitation on the product state distribution yields further insights into the reaction mechanism. In his quasiclassical trajectory study, Schatz[24] found that for both vibrationally excited OH and H_2 the excess energy is deposited preferentially in the H_2O vibrational degrees of freedom. Virtually no energy is transferred to product transiational motion, and very little to rotational degrees of freedom. The distribution of the energy among the H_2O vibrational degrees of freedom is even more intriguing. For vibrationally excited H_2 Schatz observed a nonspecific distribution of energy among the modes: with 42% going into the symmetric stretch mode, 35% into the asymmetric stretch mode and 22% into the bending mode. When the OH is initially excited, all of the excess energy goes into the OH stretching modes: 75% to the asymmetric stretch and 25% to the symmetric stretch. None of the excess energy flows into the bending mode.

The reaction path approach presented here provides a framework in which to understand this observation. In the case of H_2 excitation, there is strong coupling between the H_2 stretch and the reaction path in the entrance channel and the excess energy can flow into the reaction path. In the exit channel the energy can flow from the reaction path into the symmetric and asymmetric stretch modes as well as into the bend mode, since all three modes exhibit strong coupling with the reaction path (see Fig. 8 and Ref. 26). The net result is a nonspecific energy distribution among the product vibrational modes. For initial OH excitation, since there is little coupling between the OH stretch and the reaction path, the excess energy is confined to the

OH stretching mode which correlates (in the normal mode description) with the asymmetric stretch in the products. In the exit channel there is, however, strong coriolis coupling between the two stretching motions of the product molecule, allowing some excess energy to flow from the asymmetric stretch into the symmetric stretch. Since there is no coupling between the asymmetric stretch and the bend, none of the excess energy is deposited in the bending mode of the products.

ACKNOWLEDGMENTS

We wish to thank our colleagues, Drs. Albert F. Wagner, George C. Schatz and Lawrence B. Harding for enumerable helpful discussions. The calculations on the Li + HF reaction were carried out with a preliminary version of the reaction path program written by Dr. Harding. This work was supported by the Chemical Sciences Division of the Office of Basic Energy Sciences, U.S. Department of Energy under contract W-31-109-ENG-38.

REFERENCES

[1] G. L. Hofacker, Z. *Naturforsch. A*, 1963, **18**, 607; S. F. Fischer, G. L. Hofacker, and R. Seiler, *J. Chem. Phys.*, 1969, **51**, 3951.

[2] R. A. Marcus, *J. Chem. Phys.*, 1966, **45**, 4493, 4500; 1968, **49**, 2610.

[3] K. Fukui, *J. Phys. Chem.*, 1970, **74**, 4161.

[4] See, *e.g.*, (a) A. Tachibana and K. Fukui, *Theoret. Chim. Acta (Berl.)*, 1978, **49**, 321; (b) A. Tachibana and K. Fukui, *Theoret. Chem. Acta (Berl.)*, 1980, **57**, 81; (c) K. Fukui, A. Tachibana and K. Yamashita, *Intern. J. Quantum Chem.: Quantum Chemistry Symposium*, 1981, **15**, 621; (d) K. Fukui, *Intern. J. Quantum Chem.: Quantum Chemistry Symposium*, 1981, **15**, 633.

[5] See, *e.g.*, K. Yamashita, T. Yamabe and K. Fukui, *Chem. Phys. Lett.*, **84**, 123; K. Yamashita, T. Yamabe and K. Fukui, *Theoret. Chim. Acta (Berl.)*, 523, **60**, 1982; T. Yamabe, M. Koizumi, K. Yamashita and A. Tachibana, *J. Amer. Chem. Soc.*, 1984, **106**, 2255.

[6] W. H. Miller, N. C. Handy and J. E. Adams, *J. Chem. Phys.*, 1980, **72**, 99.

[7] J. T. Hougen, P. R. Bunker, and J. W. C. Johns, *J. Mol. Spectrosc.*, 1970, **34**, 136.

[8] Early applications include S. K. Gray, W. H. Miller, Y. Yamaguchi and H. F. Schaefer III, *J. Chem. Phys.*, 1980, **73**, 2733; Y. Osamura, H. F. Schaefer III, S. K. Gray and W. H. Miller, *J. Amer. Chem. Soc.*, 1981, **103**, 1904; B. A. Waite, S. K. Gray and W. H. Miller, *J. Chem. Phys.*, 1983, **78**, 259.

[9] For a collection of recent work in this area, see *Geometrical Derivatives of Energy Surfaces and Molecular Properties*, edited by P. Jorgensen and J. Simons (Reidel, Dordrecht, 1986).

[10] See, *e.g.*, LSODA - *Livermore Solver for Ordinary Differential Equations*, (with automatic method switching for stiff and non-stiff problems), L. R. Petzold and A. C. Hindmarsch (Sandia National Laboratory, Livermore, CA, 1985).

[11] The three translations and the three rotations are projected out by using the

center-of-mass and Eckart constraints; see Ref. 6.

[12] For a review of variational effects on chemical reactions, see D. G. Truhlar, A. D. Isaacson and B. C. Garrett, in *Theory of Chemical Reaction Dynamics. Volume IV*, edited by M. Baer, (CRC Press, Inc, Boca Raton, FL, 1985), p.65.

[13] R. A. Eades and T. H. Dunning, Jr., *to be published.*

[14] E. H. Taylor and S. Datz, *J. Chem. Phys.*, 1955, **23**, 1711.

[15] D. Herschbach, *Adv. Chem. Phys.*, 1966, **10**, 319.

[16] (a) G. G. Balint-Kurti and R. Yerdley, *Faraday Disc. Chem. Soc.*, 1977, **62**, 77; (b) M. M. L. Chen and H. F. Schaefer III, *J. Chem. Phys.*, 1980, **72**, 4376.

[17] C. H. Becker, P. Casavecchia, P. W. Tiedemann, J. J. Valentini and Y. T. Lee, *J. Chem. Phys.*, 1980, **73**, 2833.

[18] T. J. Odiorne, P. R. Brooks and J. V. V. Kasper, *J. Chem. Phys.*, 1971, **55**, 1980; J. G. Pruett, F. R. Grabiner and P. R. Brooks, *J. Chem. Phys.*, 1975, **63**, 1173.

[19] E. Rosen and T. H. Dunning, Jr., *to be published.*

[20] N. J. Brown, K. H. Eberius, R. M. Fristrom, K. H. Hoyermann and H. Gg. Wagner, *Combustion Flame*, 1978, **33**, 151.

[21] J. Warnatz, *Sandia National Laboratories Report No. SAND83-8606* (Livermore, CA, 1983)

[22] (a) J. E. Spencer, H. Endo and G. P. Glass, *Sixteenth Symposium (International) on Combustion*, (Combustion Institute, Pittsburgh, PA, 1977), p.829; (b) G. P. Glass and B. K. Chaturvedi, *J. Chem. Phys.*, **75**, 2749 (1981).

[23] G. C. Light and J. H. Matsumoto, *Chem. Phys. Lett.*, 1978, **58**, 578.

[24] R. Zellner and W. Steinert, *Chem. Phys. Lett.*, **81**, 568.

[25] S. P. Walch and T. H. Dunning, Jr., *J. Chem. Phys.*, 1980, **72**, 1303; G. C. Schatz and H. Elgersma, *Chem. Phys. Lett.*, 1980, **73**, 21.

[26] G. C. Schatz, *J. Chem. Phys.*, 1981, **74**, 113.

[27] D. G. Truhlar and A. D. Isaacson, *J. Chem. Phys.*, 1982, **77**, 3516.

[28] O. Rashed and N. J. Brown, *J. Chem. Phys.*, 1985, **82**, 5506.

[29] On the Walch-Dunning-Schatz-Elgersma surface Schatz[24] reported a 3.4 kcal/mol reduction in the adiabatic reaction barrier at 300°K, while Truhlar & Isaacson[25] reported a decrease of 2-3 kcal/mol at 300°K.

[30] J. E. Spencer, G. P. Glass, *Int. J. Chem. Kinet.*, 1977, **9**, 97; J. E. Spencer and G. P. Glass, *Int. J. Chem. Kinet.*, 1977, **9**, 111.

FIGURE CAPTIONS

Figure 1. Schematic representation of the saddle point, reaction path and reaction valley for a prototypical collinear triatomic system; in mass-weighted coordinates. The reaction path is calculated by following the path of steepest descent from the saddle point in mass-weighted cartesian coordinates. The reaction valley is a harmonic description of the potential energy surfaces centered on the reaction path.

Figure 2. Variation of R_{LiF}, R_{HF} and θ_{LiFH} along the reaction path for the Li + HF reaction. The black squares denote the calculated equilibrium geometries of the corresponding diatomic molecules. The vertical lines give the position of the bound complex (s = -90) and the saddle point (s = 0). For the mass-weighted coordinate system 1 $au = \sqrt{m_e}a_0$.

Figure 3. The singly occupied orbital along the reaction path for the Li + HF reaction. In the reactants this orbital is the 2s-orbital of the lithium atom; in the products it is the 1s-orbital of the hydrogen atom. The polarization induced by the charge distribution on the fluorine is evident in the plot of the orbital for the bound complex (s = -90). Charge transfer to the hydrogen atom is first evident at s ≈ -23 au. The contour interval is 0.05 au and all contours between -0.5 and 0.5 have been plotted. Negative contours are denoted by short dashed lines, positive contours by solid lines and nodal lines by long dashed lines.

Figure 4. Variation of the calculated vibrational frequencies along the reaction path for the Li + HF reaction. The black squares denote the calculated vibrational frequencies of the HF and LiF diatomic molecules.

Figure 5. Calculated classical and vibrationally adiabatic potentials for the Li + HF reaction. The dashed line is the classical potential (V_s); the upper solid line is the ground state vibrationally adiabatic potential (V_s^0); the lower solid line is the vibrationally adiabatic potential when the hydrogen fluoride is excited to its first excited state(V_s^1). The black squares denote the calculated energy defect (classical potential) and exoergicities (vibrationally adiabatic potentials) of the reaction.

Figure 6. Variation of the vibrational frequencies along the reaction path for the OH + H_2 reaction. The lowest solid curve corresponds to the in-plane wagging mode and the dashed curve to the out-of-plane wagging mode; these modes correlate with rotations in the reactants and products. The black squares denote the calculated vibrational frequencies for the reactants and products. A vertical line is plotted at the position of the saddle point (s = 0).

Figure 7. Calculated vibrationally adiabatic potentials for the ground state, $V_s(0,0)$, and vibrationally excited, $V_s(1,0)$ and $V_s(0,1)$, states for the $OH(n_{OH}) + H_2(n_{H_2})$ reaction.

Figure 8. Variation of the calculated curvature coupling terms along the reaction path for the $OH + H_2$ reaction. The solid curve corresponds to the term coupling the H_2 stretch with the path, the dashed curve to the term coupling the OH stretch with the path, and the dotted curve to the term coupling the HOH bend to the path.

Figure 9. The calculated OH and H_2 vibrational frequencies and the B_{OH,H_2} coriolis coupling term in the immediate vicinity of the avoided crossing of ω_{OH} and ω_{H_2}. The portion of the B_{OH,H_2} curve below zero is a result of *ringing* of the spline fit.

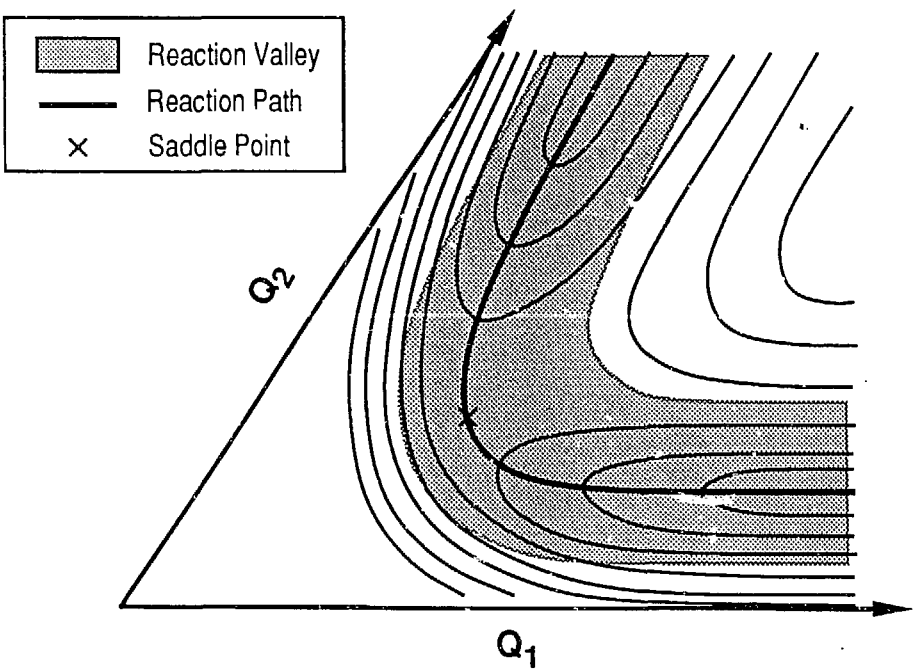
Reaction Valley
Reaction Path
Saddle Point
Q_2
Q_1

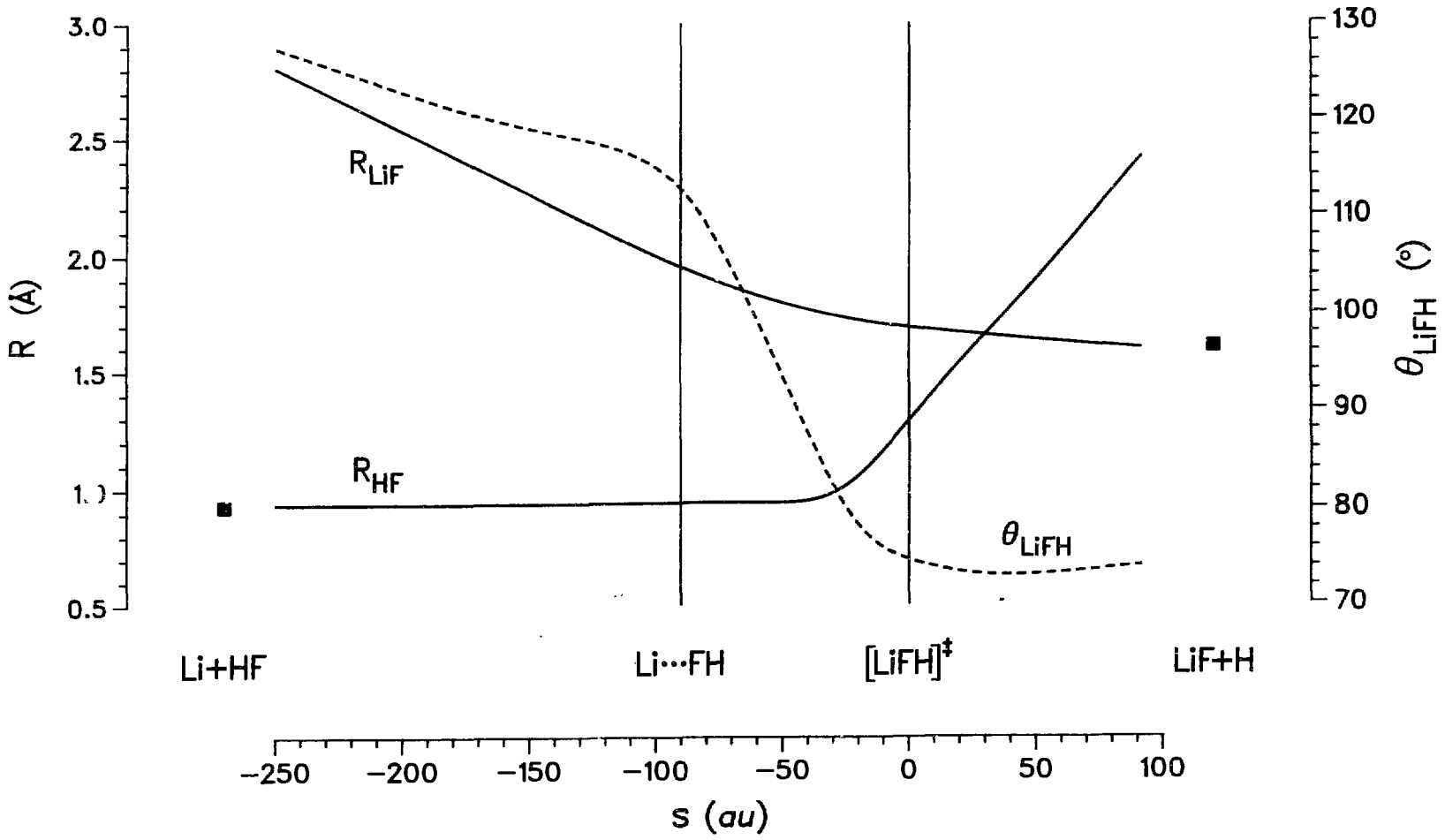
3.0
2.5
2.0
1.5
1.0
0.5
R (Å)
130
120
110
100
90
80
70
θ_{LiFH} (°)
R_{LiF}
R_{HF}
θ_{LiFH}
Li+HF
Li···FH
[LiFH]‡
LiF+H
−250
−200
−150
−100
−50
0
50
100
s (au)

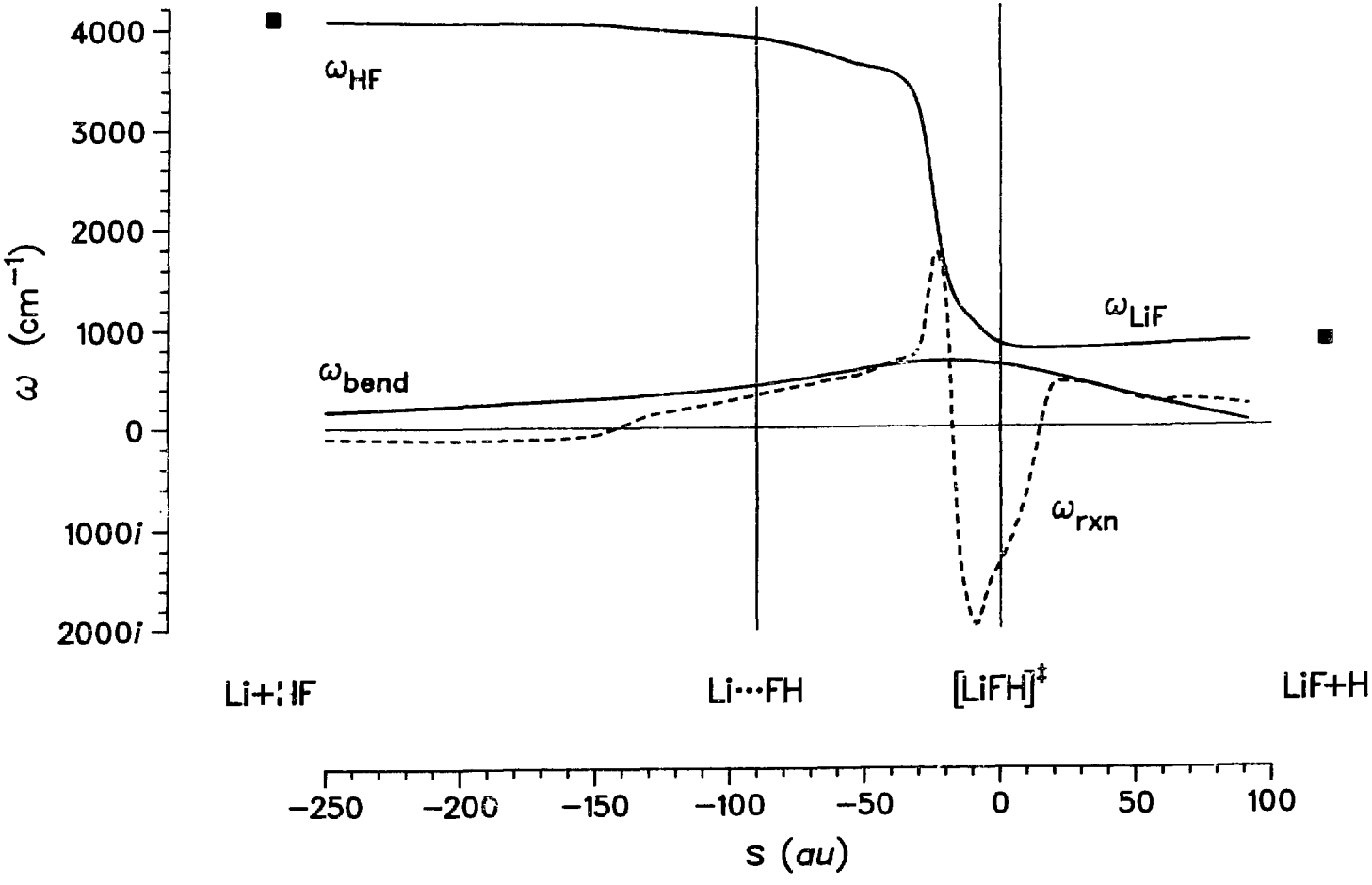
4000
3000
2000
1000
0
1000i
2000i
ω (cm⁻¹)
ωHF
ωLiF
ωbend
ωrxn
Li+HF
Li···FH
[LiFH]‡
LiF+H
−250
−200
−150
−100
−50
0
50
100
s (au)

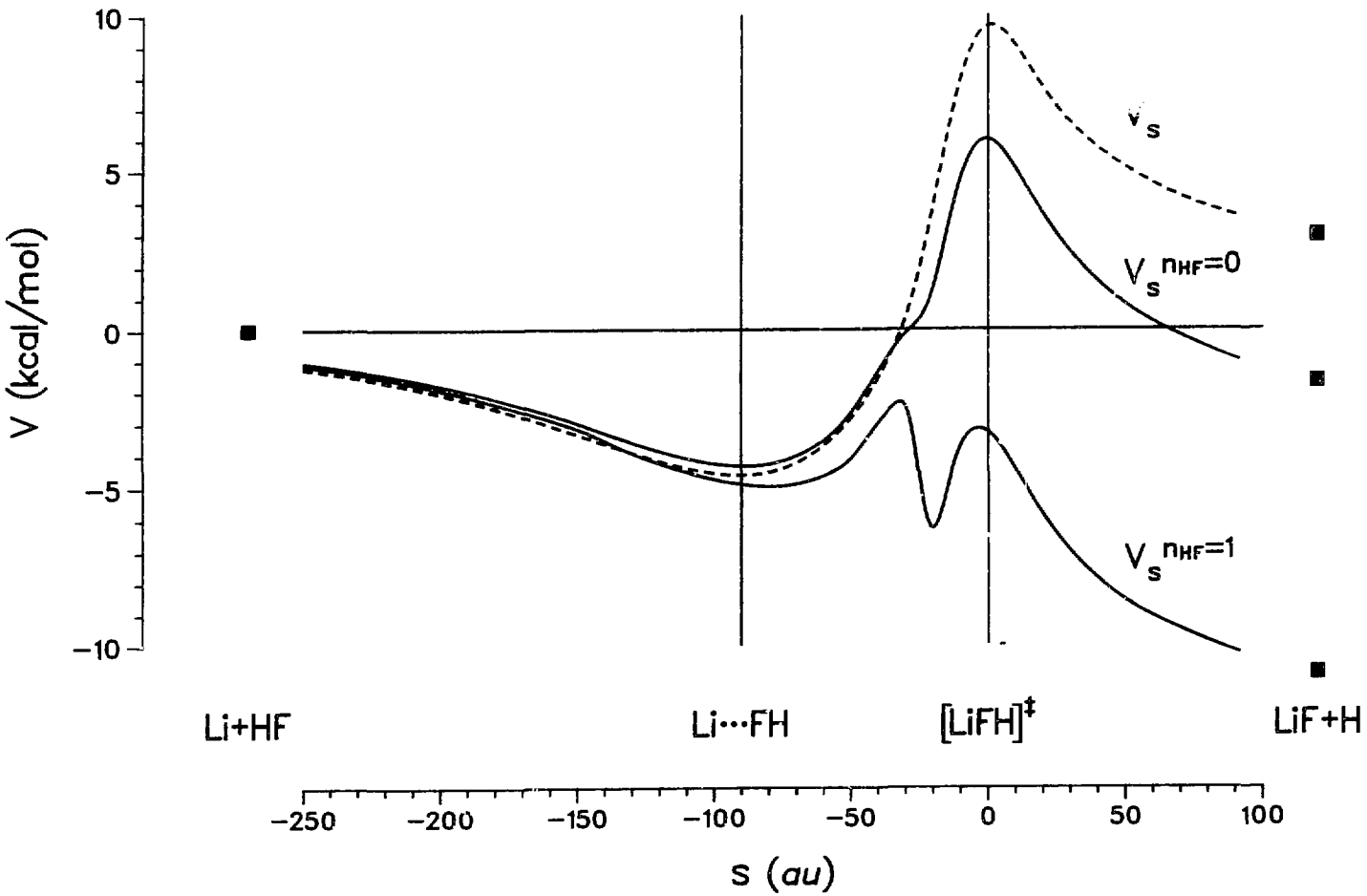
10
5
0
−5
−10
V (kcal/mol)
V_s
$V_s^{n_{HF}=0}$
$V_s^{n_{HF}=1}$
Li+HF
Li···FH
[LiFH]‡
LiF+H
−250
−200
−150
−100
−50
0
50
100
s (au)

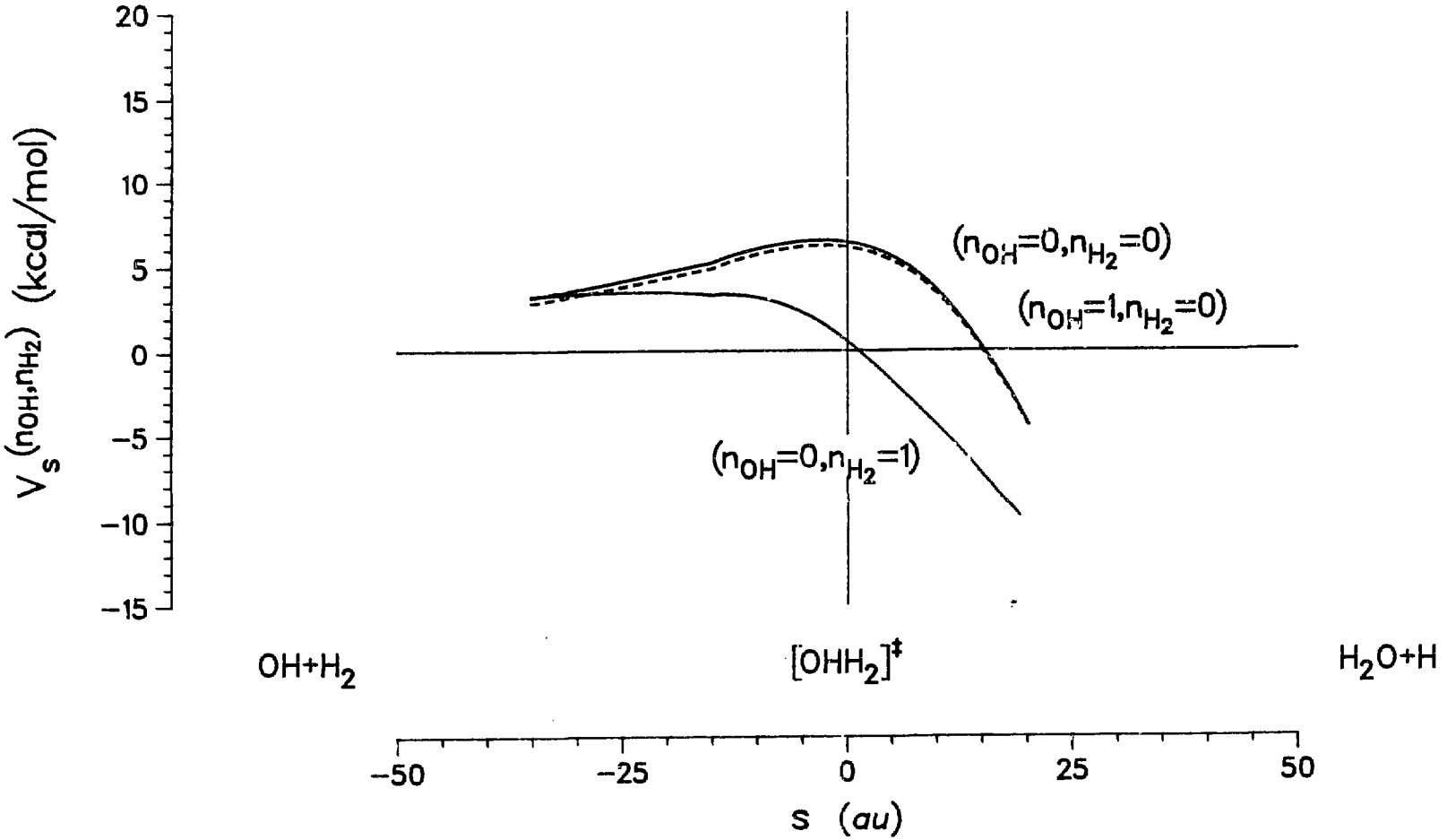
20
15
10
5
0
−5
−10
−15
$V_s(n_{OH},n_{H_2})$ (kcal/mol)
$(n_{OH}=0,n_{H_2}=0)$
$(n_{OH}=1,n_{H_2}=0)$
$(n_{OH}=0,n_{H_2}=1)$
$OH+H_2$
$[OHH_2]^{\ddagger}$
H_2O+H
−50
−25
0
25
50
s (au)

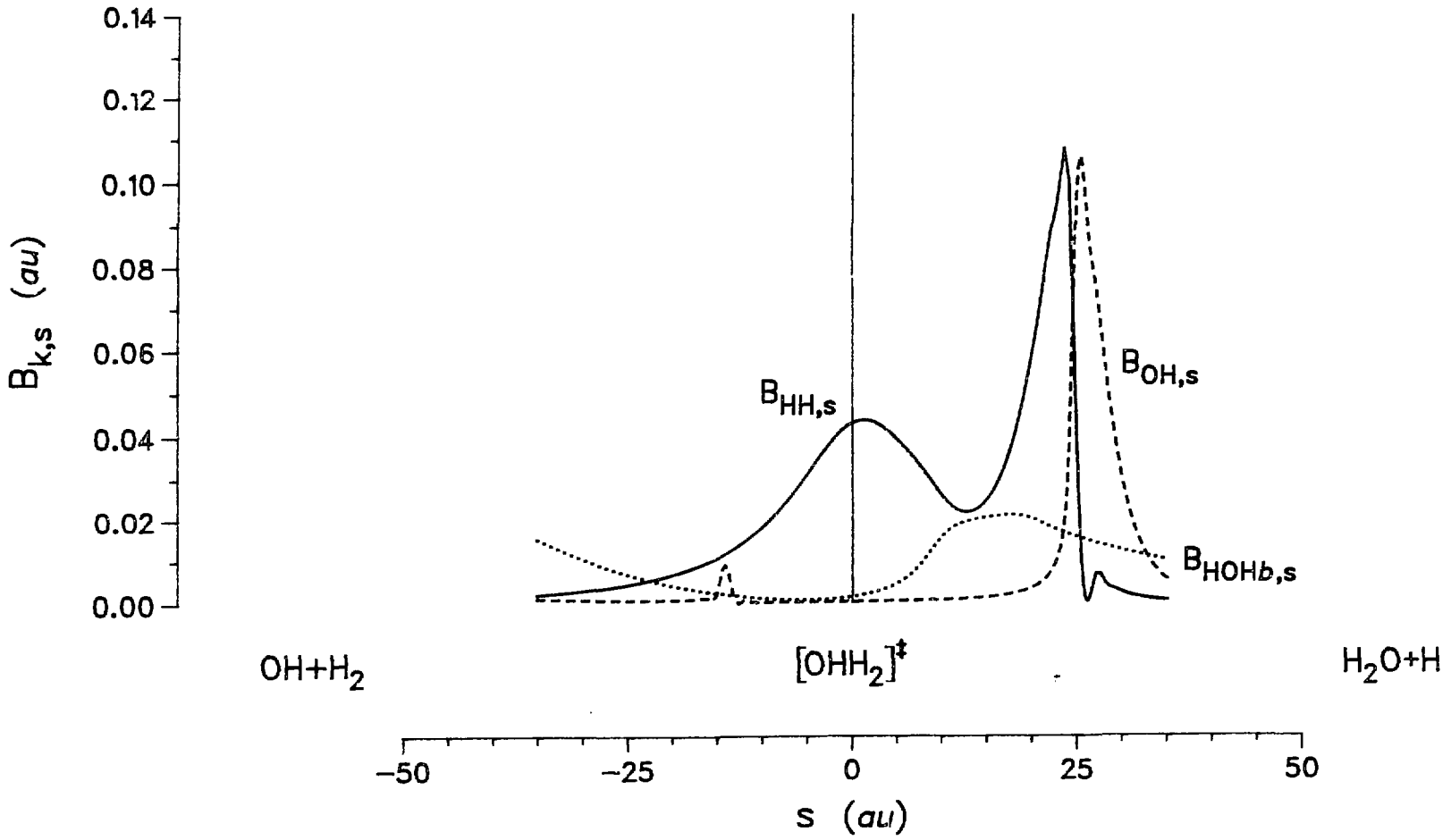
0.14
0.12
0.10
0.08
0.06
0.04
0.02
0.00
$B_{k,s}$ (au)
$B_{HH,s}$
$B_{OH,s}$
$B_{HOHb,s}$
$OH+H_2$
$[OHH_2]^{\ddagger}$
H_2O+H
−50
−25
0
25
50
s (au)

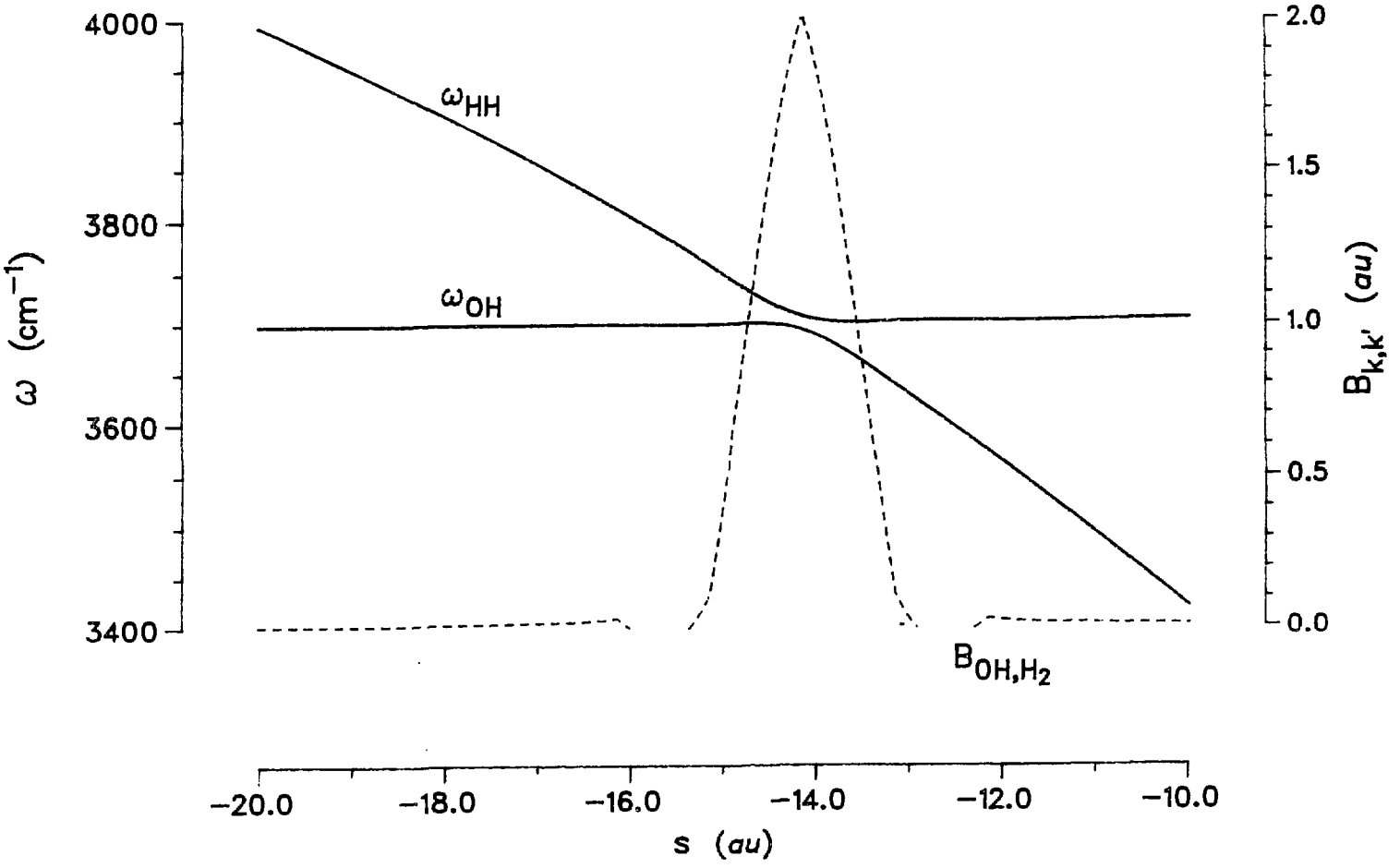
4000
3800
3600
3400
ω (cm⁻¹)
ωHH
ωOH
2.0
1.5
1.0
0.5
0.0
Bk,k' (au)
BOH,H2
−20.0
−18.0
−16.0
−14.0
−12.0
−10.0
s (au)